Thermal expansion behaviour of Long-Period Stacking Ordered (LPSO) phase

Gerardo Garcés[a,✉], Guillermo Requena[b,c], Domonkos Tolnai[d], Pablo Pérez[a],
Paloma Adeva[a], José A. Jiménez[a], Andreas Stark[d], Norbert Schell[e]

[a]Department of Physical Metallurgy, National Center for Metallurgical Research
(CENIM-CSIC), Avda. Gregorio del Amo 8, 28040 Madrid, Spain
[b]Institute of Materials Research, German Aerospace Centre, Linder Höhe, 51147 Köln, Germany
[c]RWTH Aachen, 52056 Aachen, Germany
[d]Institute of Materials Research, Helmholtz-Zentrum Geesthacht, Max-Planck-Str. 1, 21502 Geesthacht, Germany
[e]Structural Research on New Materials, Helmholtz-Zentrum Geesthacht Outstation at DESY in Hamburg, Germany
[✉]Corresponding author: ggarces@cenim.csic.es

ABSTRACT: The lineal thermal expansion coefficient of the 18R Long-Period Stacking Ordered (LPSO) structure was determined in the range between room temperature and 400 °C by dilatometry and synchrotron radiation diffraction. Results clearly show that the lineal thermal expansion coefficients for magnesium and the LPSO phase are similar and therefore no mismatch thermal stresses are generated at their interface in two-phase Mg-Y-Zn alloys containing this phase during thermomechanical processing.

KEYWORDS: Magnesium alloys; LPSO phase; Synchrotron radiation diffraction; Thermal expansion coefficient

RESUMEN: *Coeficiente de dilatación térmica de la fase LPSO*. El coeficiente lineal de expansión térmica de la fase LPSO con estructura cristalográfica 18R se determinó en el intervalo entre temperatura ambiente y 400 °C mediante dilatometría y difracción de radiación sincrotrón. Los resultados muestran claramente que el coeficiente lineal de dilatación térmica de las fases magnesio y LPSO son similares y, por tanto, no se generan tensiones térmicas en su intercara durante el procesado termomecánico de aleaciones bifásicas Mg-Y-Zn.

PALABRAS CLAVE: Aleaciones de magnesio; Coeficiente de dilatación térmica; Difracción de radiación sincrotrón; Fase LPSO

1. INTRODUCTION

The aerospace and automotive industry is particularly interested in magnesium alloys for applications which require low density and high strength materials. Long Period Stacking Ordered Structures (LPSO) have received significant research interest in recent years as strengthening phase for Mg alloys. The reinforcing effect of LPSO structures in extruded Mg-Y-Zn alloys is due to a load transfer mechanism from the magnesium matrix to the stiffer LPSO phase. The Young's modulus of the LPSO phase is higher than that of the magnesium matrix (Oñorbe *et al.*, 2011; Oñorbe *et al.*, 2012; Tane *et al.*, 2014)

and, therefore, these alloys behave mechanically as a metal matrix composite. The reinforcing effect of the LPSO phase in the extruded alloys is effective up to temperatures below 250 °C (Oñorbe *et al.*, 2012).

In metal matrix composites reinforced with ceramic phases, mismatch stresses are generated during heating-cooling cycles and thermomechanical process used in the industrial manufacturing, due to significant differences between the thermal expansion coefficients of the metal matrix and the ceramic reinforcement (normally around one order of magnitude) (Clyne and Whithers, 1993). These mismatch stresses are mainly localized in the vicinities of matrix/reinforcement interfaces and their sign and magnitude depend on the shape and size of the reinforcement, the CTE-mismatch between the components and eventual relaxation mechanisms acting in the matrix (Requena *et al.*, 2012). Ultimately, a large build-up of internal stress may lead to unexpected and dramatic failure. Since the presence of residual stresses may lead to fracture at lower loads than might be expected and originate difficulties during cold working or forming.

In aluminium matrix composite is has been reported that residual stress induces a tension-compression asymmetry where yield stress in compression is higher than in tension (Arsenault and Taya, 1987). This fact is caused by the development of compressive residual stress during the composite processing. In magnesium matrix composites, this effect is masked by the crystallographic texture. Although, compressive residual stresses have been also reported using synchrotron diffraction (Garcés *et al.*, 2009; Garcés *et al.*, 2011). In magnesium alloys containing a high volume fraction of LPSO elongated fibers, Hagihara *et al.* (2010a) showed that the Mg-7Y-2Zn (wt.%) alloy exhibited a higher yield stress in compression than in tension. The existence of residuals stress between LPSO and magnesium matrix could explain this rare behaviour in magnesium alloys.

In the literature, however, almost no data are available on the thermal expansion coefficient of the LPSO phase in Mg-Zn-RE alloys. The alloy Mg-11Y-5Gd-2Zn-0.5Zr (wt.%) alloy containing LPSO particles shows an average linear thermal expansion coefficient of 2.94×10^{-5} K^{-1} (Chen *et al.*, 2009). This paper evaluates the linear CTE of the LPSO phase using two different techniques, dilatometry and synchrotron diffraction from room temperature to 400 °C, to confirm the existence of compressive residual stresses.

2. MATERIALS Y METHODS

The Mg$_{97}$Y$_7$Zn$_5$(at.%) alloy used for this study was prepared by melting high purity elements Mg, Y and Zn and Mg-22%Y(wt.%) master alloys in a graphite crucible coated with boron nitride under a protective atmosphere of argon. X ray fluorescence analysis revealed that the chemical composition of this alloy was almost the same as the nominal composition. The fully LPSO alloy was homogenized at 350 °C for 24 hours.

Microstructural characterization of the alloys was carried out by scanning electron microscopy (SEM) and transmission electron microscopy (TEM). Metallographic preparation for optical and SEM observation consisted of mechanical polishing and etching in a solution of 0.5 g picric acid, 5 ml acetic acid, 20 ml ethanol, 1ml water and 25 ml methanol. Specimens for TEM observation were prepared by electrolytic polishing using a reactive mixture of 25% nitric acid and 75% methanol at −30 °C and 20 V. Then, ion milling at liquid nitrogen temperature was used to remove the fine oxide film formed on the surface during electrolytic polishing.

Dilatometry was carried out using a Bähr DIL805A dilatometer. Two samples with a diameter of 5 mm and a length of 10 mm were heated by an induction coil. Three heating-cooling cycles between room temperature and 500 °C were applied using a heating/cooling rate of 5 K min^{-1}. The temperature was monitored using a K thermocouple welded at the centre of the sample. The change in length was measured using an LVDT with an accuracy of 50 nm. The first heating/cooling cycle was disregarded for the calculation of the linear CTE since it may exhibit the effect of relaxation of stresses introduced during production of the material. The measurements where calibrated using a Pt sample subjected to the same heating-cooling cycles as the alloy.

High energy synchrotron radiation diffraction was performed at the P07-HEMS beamline of PETRA III, at the Deutsches Elektronen-Synchrotron (DESY). Cylinders of 10 mm of length and 5 mm in diameter were heated using the induction coil of a Bähr DIL805D dilatometer. The measurements were performed under flowing argon. High energy synchrotron radiation diffraction was necessary to acquire simultaneously several reflections of the LSPO phase. The diffraction patterns were recorded using an exposure time of 1 second by a Perkin-Elmer XRD 1622 flatpanel detector with an array of 20482 pixels, with an effective pixel size of 200×200 μm^2. The beam energy was 100 keV corresponding to a wavelength of 0.0124 nm. LaB$_6$ was used as a reference to calibrate the acquired diffraction spectra. The detector-to-sample distance was 1918.95 mm. Conventional line profiles were obtained by azimuthal integration of the Debye-Scherrer rings using the software Fit2D (Hammersley *et al.*, 1996). Diffraction patterns were obtained at room temperature, 100 °C, 200 °C and 300 °C. The samples were maintained at each temperature 300 seconds before the acquisition of diffraction patterns to homogenize the temperature.

Integrated diffraction patterns were interpreted fitting the whole pattern with the version 4.2 of

the analysis program TOPAS (Bruker AXS) by using the LeBail's method. In this approach, the superposition of analytical line-profile functions describing each Bragg reflection, and a suitable background model, are fitted to the observed data by a non-linear squares algorithm for the calculation of structural parameters of crystalline phases. In practice, it is necessary to refine simultaneously background functions, peak shapes and lattice parameters. The background was approximated by means of Chevyshev polynomial of 2nd order and some additional pseudo-Voigt functions to fit the background associated with the direct beam stop and air scattering, Compton scattering and thermal diffuse scattering. The peak shape data were modeled with high accuracy by using the approximation provided by the Thompson-Cox-Hastings pseudo-Voigt function (Thompson *et al.*, 1987). Finally, the structure used in the refinement was the 18R-type LSPO phase ($P3_212$ space group) with the initial cell dimensions reported by Egusa and Abe (2012).

3. RESULTS AND DISCUSSION

Figure 1 shows the microstructure of the as-cast $Mg_{89}Y_7Zn_5$ alloy. It consists mainly of long LPSO laths, which are randomly oriented, with a small volume fraction of the magnesium phase with a dark contrast. This microstructure is in agreement with previous studies of the same alloy (Hagihara *et al.*, 2010b; Garcés *et al.*, 2014a; Garcés *et al.*, 2014b). As the volume fraction of LPSO phase, estimated from 10 images similar to Fig. 1 is 96.8±0.2 vol%, our polycrystal alloy was quite suitable for the analysis of the thermal expansion coefficient in the 18R LPSO phase. The microstructure of this alloy was analyzed by TEM to confirm that the LPSO phase consisted of a 18R structure, which it has been indexed by the hexagonal notation by considering
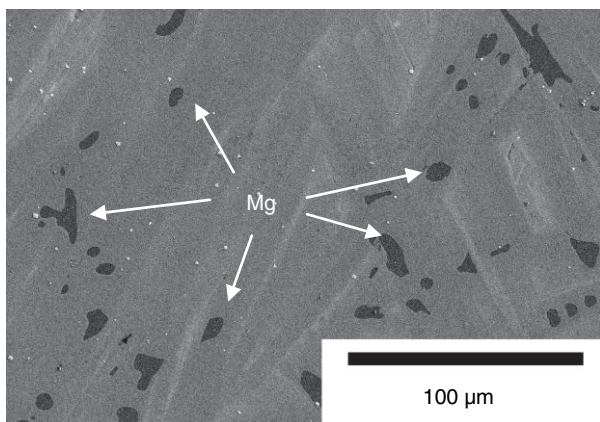
a unit cell with a volume three times larger than that of the rhombohedral cell. Figure 2a shows a TEM image of the LPSO phase in the $Mg_{97}Y_7Zn_5$ alloy at the $\langle 11\bar{2}0 \rangle_\alpha$ zone axis when the (0002) g is excited. The LPSO crystal structure can be identified through the Selected Area Electron Diffraction pattern (SAED) at the $\langle 11\bar{2}0 \rangle_\alpha$ zone axis or by measuring the fringe spacing in the [0002] direction formed when the g (0002) is excited. The SAED pattern (Fig. 2b) and the fringe spacing of 1.6 nm confirms the 18R structure.

Figure 3a shows the Debye-Scherrer rings obtained at room temperature. The integration of the Debye-Scherrer rings to obtain the diffraction patterns as a function of 2θ has been carried out using the software Fit2D (Hammersley *et al.*, 1996). Figure 3b shows the indexed 2θ diffraction patterns for the $Mg_{89}Y_7Zn_5$ alloy. The crystal structure of the LPSO phase in the cast $Mg_{89}Y_7Zn_5$ alloy corresponds to the 18R structure, in agreement with TEM observation, which can be clearly distinguished by the 0003 diffraction peak located at 2θ=0.44°. Other diffraction peaks overlap 18R and 14H structures. As stated in the introduction section, the LeBail method was used to analyze the XRD pattern of as cast samples considering a 18R trigonal lattice (space group $P3_212$) as initial structural model. The complexity of this refinement arises from the large primitive unit cell of the material, which results in near 1000 Bragg reflections possible between 0 and 5.6° when using synchrotron radiation with a wavelength of 0.124 Å. A visual examination of Le Bail refinement of a pattern obtained at room temperature indicates a good fit, as shown in Fig. 3c.

Figure 4 shows the relative change in length during the second heating cycle of one of the samples measured by dilatometry. The third cycle shows the same behaviour and it has been omitted to improve legibility. The same is valid for the second and the third cycle of a second sample. The slope of this curve between RT (Room Temperature) and 400 °C gives the linear CTE
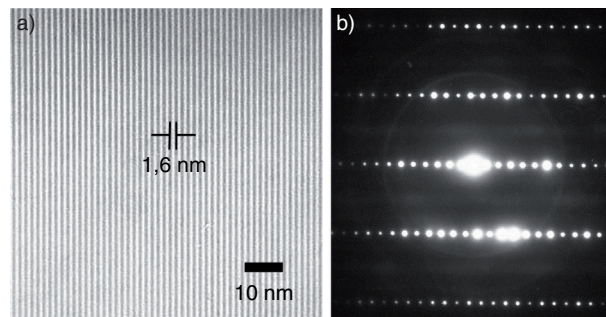

FIGURE 1. Microstructure of the cast MgY_7Zn_5 (at.%) alloy. (White arrows indicate the magnesium islands).

FIGURE 2. a) Bright field TEM image of the LPSO phase in the cast MgY_7Zn_5 (at.%) alloy [B=$\langle 11\bar{2}0 \rangle$ and g=(0002)]. b) Selected area diffraction pattern of the LPSO phase at the $\langle 11\bar{2}0 \rangle$ zone axis.
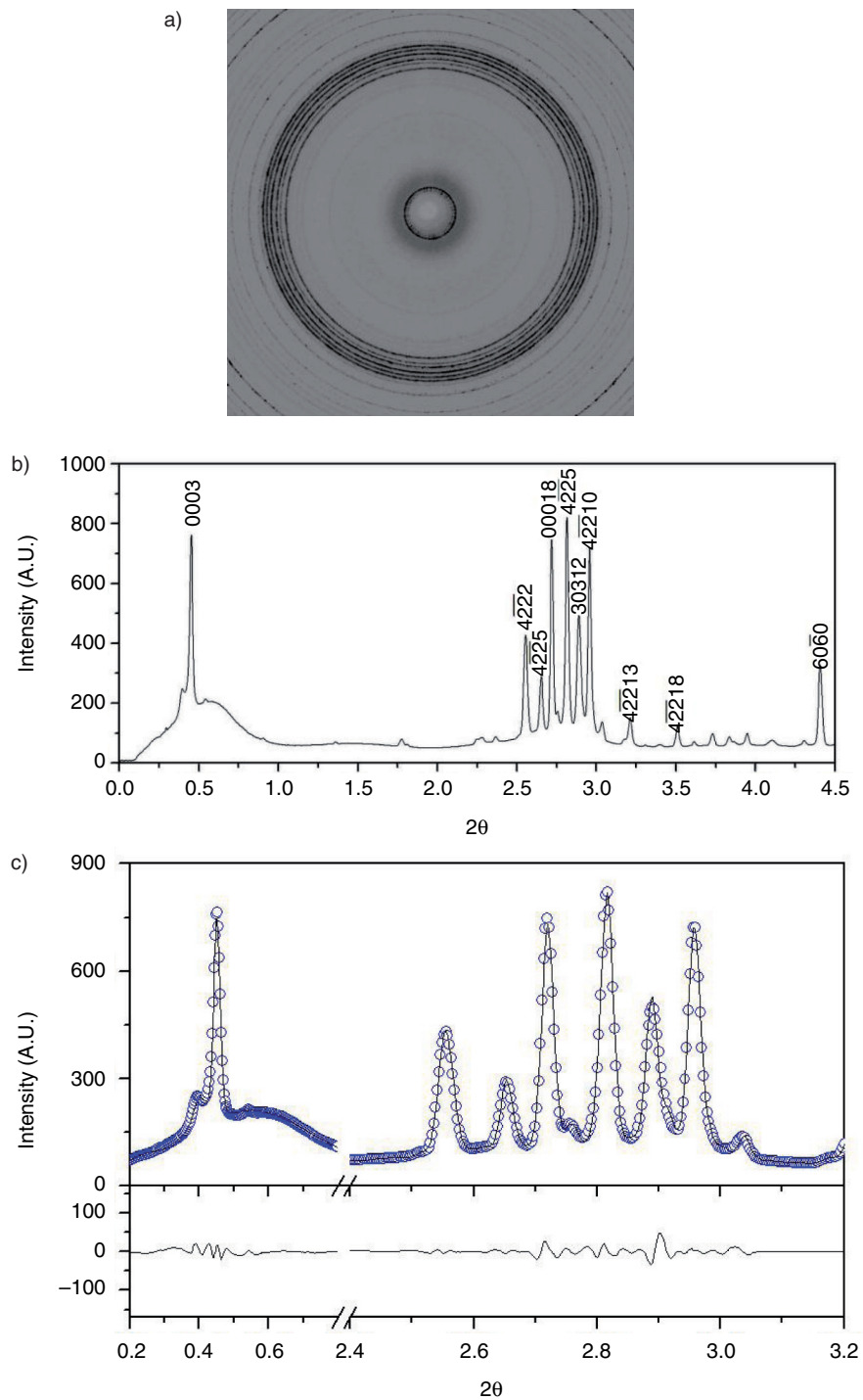
FIGURE 3. Synchrotron diffraction patterns at room temperature of the cast MgY$_7$Zn$_5$ (at.%) alloy: a) obtained from the 2D detector, b) as a function of 2θ and c) Le Bail refinement of the 2θ diffraction pattern.

value of the Mg$_{89}$Y$_7$Zn$_5$ alloy in this temperature range. The linear CTE between RT and 400 °C obtained as the mean value from the second and third cycle of both samples is 2.7×10^{-5} K^{-1}. This is the linear CTE of the alloy, i.e. it reflects the combined effect of ~97 vol% of the 18R LPSO phase and ~3 vol% of α-Mg. In order to separate the CTE value of the LPSO phase, it is necessary to use an alternative method which can evaluate this phase individually. Therefore, the linear CTE of the 18R LPSO phase was estimated considering the evolution of its lattice parameter with
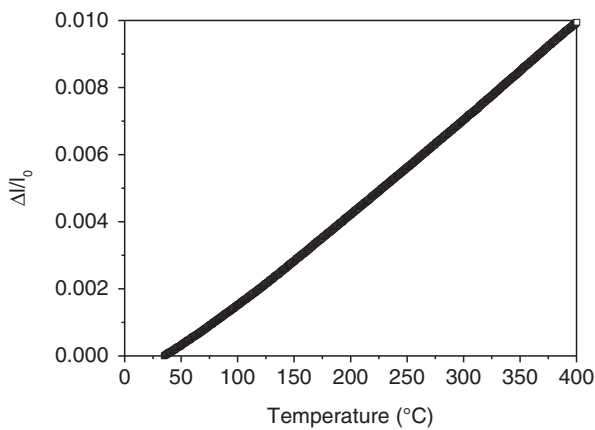
FIGURE 4.   Relative change in length of the cast MgY$_7$Zn$_5$ (at.%) alloy during heating to 400 °C.
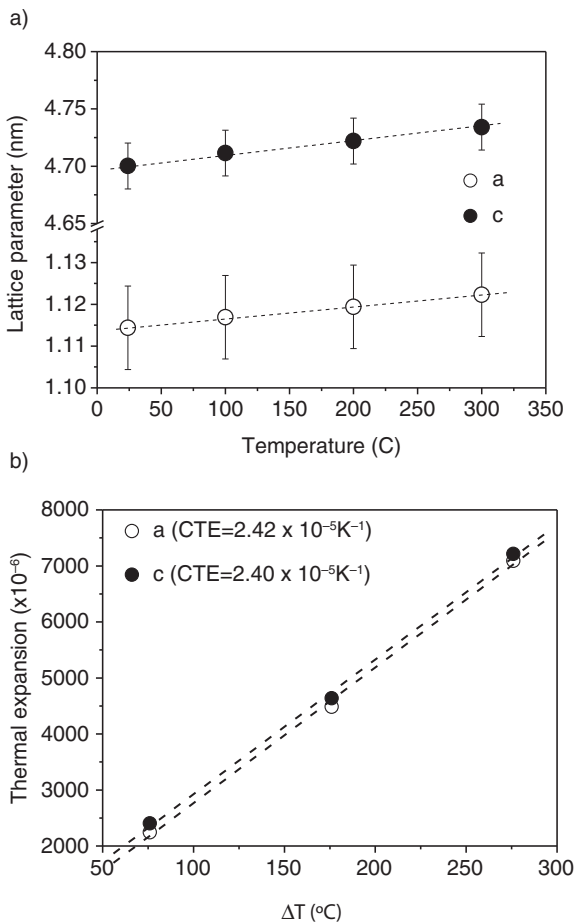
a)

b)

FIGURE 5.   a) Evolution of lattice parameters, a and c, of the LPSO phase as a function of temperature. b) Changes of lattice parameters, a and c, of the LPSO phase as function of temperature.

temperature from the diffraction patterns. The evolution of a and c values with temperature have been calculated fitting the diffraction pattern from

RT to 300 °C (Fig. 5a). Lattice parameters of the 18R LPSO phase at room temperature are in agreement with previous references (Garcés *et al.*, 2014a; Garcés *et al.*, 2014b) and increase with temperature as expected. The linear CTE for the lattice parameters, a and c, α, can be calculated from (Eq. 1):

$$\alpha_{lattice} = \frac{1}{d_0}\left(\frac{\Delta d}{\Delta T}\right) \qquad (1)$$

where d_0 is the lattice parameter at room temperature. Figure 5b shows the thermal elastic expansion $\frac{\Delta d}{d_0}$, as a function of the temperature increment. The slope of this curve gives directly the linear CTE for each lattice parameter. CTE values are 2.42×10^{-5} and 2.40×10^{-5} K^{-1} for a and c lattice parameters, respectively. Values are slightly smaller than that obtained by dilatometry as well as the linear CTE of pure magnesium (2.7×10^{-5} K^{-1} (Smithells, 1992)). Nevertheless, only small thermal mismatch stresses due to differences in CTE will be generated at the Mg/LPSO interface. This fact together with the perfect epitaxy between the magnesium and LPSO phases (($0001)_{18R}$//($0001)_\alpha$ and $[10\bar{1}0]_{18R}$//$[10\bar{1}0]_\alpha$ (Yamasaki *et al.*, 2011)) explain the good quality of the interface observed during tensile deformation of extruded MgY$_{2x}$Zn$_x$ (Yamasaki *et al.*, 2010; Yamasaki *et al.*, 2013) alloys which combine high tensile strength with higher elongation compared with ceramic reinforced composites (Clyne and Withers, 1993) and other magnesium alloys.

4. CONCLUSIONS

The linear coefficient of thermal expansion of the 18R LPSO phase has been determined by dilatometry and high energy synchrotron diffraction. It has been demonstrated that the linear CTE of 18R LPSO is very similar to that of magnesium and, therefore, no thermal mismatch stresses are generated at the LPSO-Mg interface during thermal transients.

REFERENCES

Arsenault, R.J., Taya, M. (1987). Thermal residual stress in metal matrix composite. *Acta Metall.* 35, 651–659. http://dx.doi.org/10.1016/0001-6160(87)90188-X.

Clyne, T.W., Withers, P.J. (1993). *An introduction to Metal matrix composite*, Cambridge University Press, UK.

Chen, C.J., Wang, Q.D., Yin, D.D. (2009). Thermal properties of Mg-11Y-5Gd-2Zn-0.5Zr (wt.%) alloy. *J. Alloys Comp.* 487, 560–563. http://dx.doi.org/10.1016/j.jallcom.2009.07.177.

Egusa, D., Abe, E. (2012). The structure of long period stacking/order Mg-Zn-RE phases with extended non-stoichiometry ranges. *Acta Mater.* 60, 166–178. http://dx.doi.org/10.1016/j.actamat.2011.09.030.

Garcés, G., Oñorbe, E., Pérez, P., Denks, I.A., Adeva, P. (2009). Evolution of internal strain during plastic deformation in magnesium matrix composites. *Mat. Sci. Eng. A* 523, 21–26. http://dx.doi.org/10.1016/j.msea.2009.06.026.

Garcés, G., Oñorbe, E., Pérez, P., Klaus, M., Genzel, C., Adeva, P. (2011). Influence of SiC particles on compressive deformation of magnesium matrix composites. *Mat. Sci. Eng. A.* 533, 119–123. http://dx.doi.org/10.1016/j.msea.2011.10.103.

Garcés, G., Requena, G., Tolnai, D., Pérez, P., Adeva, P., Stark, A., Schell, N. (2014a). Influence of rare-earth addition on the long-period stacking ordered phase in cast Mg-Y-Zn alloys. *J. Mater. Sci.* 49, 2714–2722. http://dx.doi.org/10.1007/s10853-013-7967-4.

Garcés, G., Muñoz-Morris, M.A., Morris, D.G., Jiménez, J.A., Pérez, P., Adeva, P. (2014b). The role of extrusion texture on strength and its anisotropy in a Mg-base alloy composed of the Long-Period-Structural-Order phase. *Intermetallics* 55, 167–176. http://dx.doi.org/10.1016/j.intermet.2014.07.015.

Hagihara, K., Kinoshita, A., Sugino, Y., Yamasaki, M., Kawamura, Y., Yasuda, H.Y., Umakoshi, Y. (2010a). Plastic deformation behavior of Mg97Zn1Y2 extruded alloys. *T. Nonferr. Metal. Soc.* 20, 1259–1268. http://dx.doi.org/10.1016/S1003-6326(09)60288-0.

Hagihara, K., Yokotani, N., Umakoshi, Y. (2010b). Plastic deformation behaviour of Mg$_{12}$YZn with 18R long-period stacking ordered structure. *Intermetallics* 18, 267–276. http://dx.doi.org/10.1016/j.intermet.2009.07.014.

Hammersley, A.P., Svensson, S.O., Hanfland, M., Fitch, A.N., Häusermann, D. (1996). Two-Dimensional Detector Software: From Real Detector to Idealised Image or Two-Theta Scan. *High Pressure Res.* 14, 235–248. http://dx.doi.org/10.1080/08957959608201408.

Oñorbe, E., Garcés, G., Pérez, P., Cabeza, S., Klaus, M., Genzel, C., Frutos, E., Adeva, P. (2011). The evolution of internal strain in Mg-Y-Zn alloys with a long period stacking ordered structure. *Scr. Mater.* 65, 719–722. http://dx.doi.org/10.1016/j.scriptamat.2011.07.017.

Oñorbe, E., Garcés, G., Pérez, P., Adeva, P. (2012). Effect of the LPSO volume fraction on the microstructure and mechanical properties of Mg-Y$_{2x}$-Zn$_x$ alloys. *J. Mater. Sci.* 47, 1085–1093. http://dx.doi.org/10.1007/s10853-011-5899-4.

Requena, G., Canelo Yubero, D., Corrochano, J., Repper, J., Garcés, G. (2012). Stress relaxation during thermal cycling of particle reinforced aluminium matrix composites. *Comp. A* 43, 1981–1988. http://dx.doi.org/10.1016/j.compositesa.2012.07.004.

Smithells (1992). *Metals Reference Book* Chapter 14–19, Edited by E.A. Brandesnad G.B. Brook Butterworth-Heinemann Ltd Linacre House, Oxford.

Tane, M., Nagai, Y., Kimizuka, H., Hagihara, K., Kawamura, Y. (2014). Elastic properties of an Mg-Zn-Y alloy single crystal with a long-period stacking-ordered structure. *Acta Mater.* 59, 6338–6351. http://dx.doi.org/10.1016/j.actamat.2013.06.041.

Thompson, P., Cox, D.E., Hastings, J.B. (1987). Rietveld refinement of Debye-Scherrer synchrotron X-ray data from Al$_2$O$_3$. *J. Appl. Crystallogr.* 20, 79–83. http://dx.doi.org/10.1107/S0021889887087090.

Yamasaki, M., Hashimoto, K., Hagigara, K., Kawamura, Y. (2010). Multimodal Microstructure Evolution in Wrought Mg-Zn-Y Alloys with High Strength and Increased Ductility. *Mater. Sci. Forum* 654–656, 615–618.

Yamasaki, M., Hashimoto, K., Hagihara, K., Kawamura, Y. (2011). Effect of multimodal microstructure evolution on mechanical properties of Mg-Zn-Y extruded alloy. *Acta Mater.* 59, 3646–3658. http://dx.doi.org/10.1016/j.actamat.2011.02.038.

Yamasaki, M., Hagihara, K., Inoue, S., Hardorn, J.P., Kawamura, Y. (2013). Crystallographic classification of kink bands in an extruded Mg-Zn-Y alloy using intragranular misorientation axis analysis. *Acta Mater.* 61, 2065–2076. http://dx.doi.org/10.1016/j.actamat.2012.12.026.